Marine Pollution Bulletin 129 (2018) 26–34

Contents lists available at ScienceDirect

Marine Pollution Bulletin

journal homepage: www.elsevier.com/locate/marpolbul

Effects of seasonal variations on sediment-plume streaks from dredging operations

Nam-Hoon Kim[a], Van Sy Pham[a], Jin Hwan Hwang[b,*], Nam Il Won[c], Ho Kyung Ha[d], Jungho Im[e], Youngsung Kim[c]

[a] Department of Civil and Environmental Engineering, Seoul National University, Republic of Korea
[b] Institute of Construction and Environmental Engineering, Seoul National University, Republic of Korea
[c] Korea Water Resources Corporation, Daejeon, Republic of Korea
[d] Department of Ocean Sciences, Inha University, Incheon, Republic of Korea
[e] School of Urban and Environmental Engineering, Ulsan National Institute of Science and Technology, Ulsan, Republic of Korea

ARTICLE INFO

Keywords:
Dredging
Streak
Plume
Suspended sediment
Restoring force

ABSTRACT

When mixtures of aggregates and water dredged from the seabed are discharged at the surface into the adjacent water from a barge, coarse sediments sink immediately and fine sediments are suspended forming a plume. Recently, elongated plumes of fine sediment were observed by satellites near a dredging location on the continental shelf. Such plume streaks were longer in certain conditions with seasonality than expected or reported previously. Therefore, the present work studied the appearance of sediment plume with field measurements and numerical simulations and explains the seasonally varying restoring force and thicknesses of the surface mixed layer resulting from the vertical density distribution near the surface, along with mixing by hydrodynamic process. The resulting mixtures, after vertical restoring and mixing with the surroundings, determine the horizontal transport of suspended sediments. A numerical model successfully reproduced and explained the results from field measurements and satellite images along with the seasonal variations.

1. Introduction

During mining operations of marine aggregates from the ocean bottom, significant amounts of seawater and sediments are released back to the sea from the barge. The mixture of aggregates and seawater is dredged from the seabed with hydraulic pumps, brought through pipes to the sea surface and then poured through chutes from the side of the barge. Coarser and denser sands in the mixture sink almost immediately to the seabed and are deposited near the mining site. On the other hand, fine sediments in the mixture have densities which are not enough to cause them to sink fast, resulting in suspension for a long time. Hence depending on the surrounding surface conditions, suspended sediments are expected to be able to travel several kilometers away from the dredging location (Wit et al., 2014). Such suspended sediments have potential impacts on water quality in the water column; for instance the increase in turbidity, which inhibits sunlight from penetrating deeper waters. The limited availability of light reduces primary production and vegetation on the seabed is smothered, ultimately affecting the local benthic community and habitat (Erftemeijer and Lewis III, 2006; Kim and Lim, 2007; Capello et al., 2013; Wit et al., 2014).

Therefore, the physical behaviors and concentrations of suspended sediments, with resulting turbidity, have been widely studied in relation to environmental and ecological issues, and there have been many attempts to estimate how long fine sediments can be suspended at the surface and how far they can travel away from the source. Hitherto, Lagrangian observations, such as tracing sediment clouds using a ship, have been used to study suspended sediment transport. Such Lagrangian observations, however, are limited in capturing only a narrow picture of the transport of a suspended sediment cloud in a small area for a short time period; moreover it's easy to lose track of the cloud when there is a sudden change of current direction. Hence in conventional in-situ observations, plume lengths of dredged and suspended sediments are reported to have a maximum of 11 km (Hitchcock and Drucker, 1996) and are usually no more than several kilometers (e.g., Goodwin and Michaelis, 1984; Newell et al., 1998; Battisto and Friedrichs, 2003; Kutser et al., 2007). Only in numerical simulations are plume lengths seen to develop to a maximum of 20 km from a long continuous source after one month with long-period removal of significant background disturbances (Kim and Lim, 2009).

* Corresponding author.
E-mail address: jinhwang@snu.ac.kr (J.H. Hwang).

https://doi.org/10.1016/j.marpolbul.2018.02.014
Received 3 September 2017; Received in revised form 2 February 2018; Accepted 5 February 2018
Available online 10 February 2018
0025-326X/ © 2018 The Authors. Published by Elsevier Ltd. This is an open access article under the CC BY license (http://creativecommons.org/licenses/BY/4.0/).

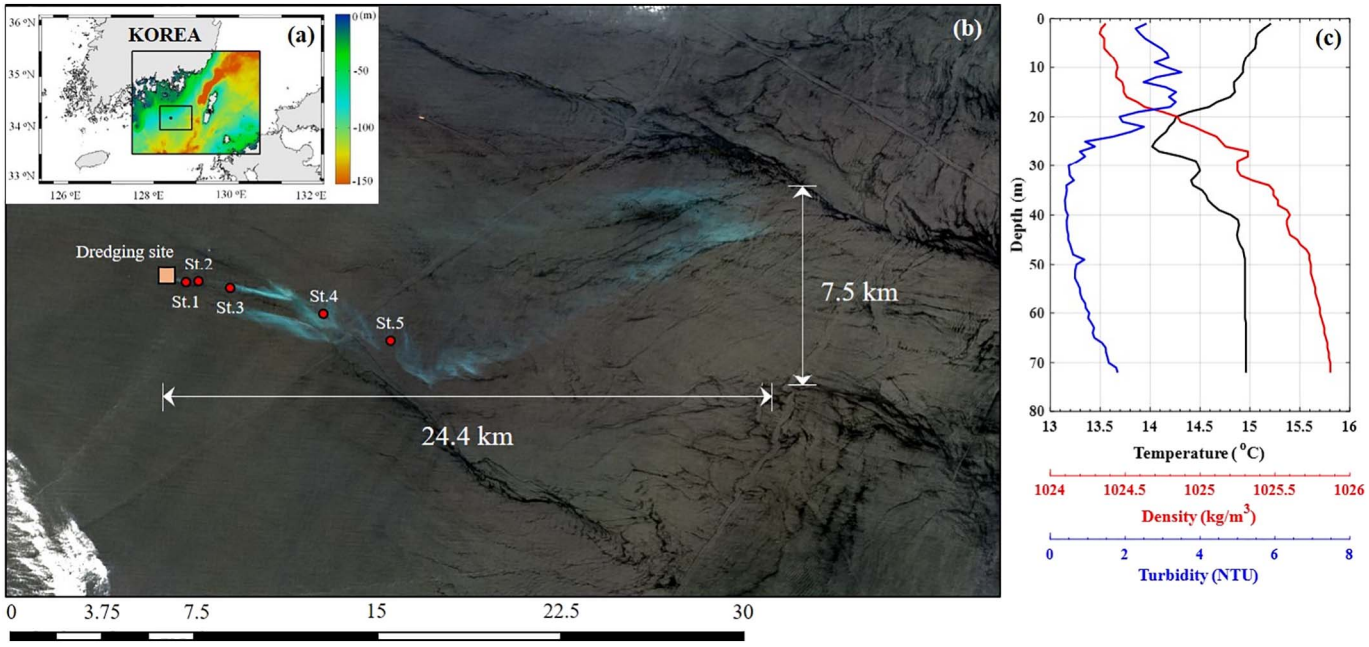

Fig. 1. (a) Geographical layout of the study area, (b) satellite image (Landsat 8) of suspended sediment plume (May 19th, 2015, 10:30 am), (c) example of field observed profiles of temperature, density and turbidity.

Table 1
Characteristics of suspended sediment plumes observed from GOCI satellite images.

	Spring (March–May)		Summer (June–August)		Autumn (September–November)		Winter (December–February)	
Longitudinal distance of suspended sediment plume	< 10 km	> 10 km	< 10 km	> 10 km	< 10 km	> 10 km	< 10 km	> 10 km
Number of suspended sediment plume	2	4	1	5	1	3		1
Total number of suspended sediment plume	6/8		6/9		4/12		1/12	
Probability for presence of the suspended sediment plume	75%		66.67%		33.33%		8.33%	

Remote observations have recently expanded suspended-sediment cloud tracking capabilities in conditions of clear visibility, and facilitated finding traces of those clouds which hitherto have not been observed well (Ali et al., 2016; Kim et al., 2014; Son et al., 2014). As an example, Landsat 8 recently captured an image of a plume streak with length over 20 km within 8–10 h of release (Fig. 1). And we found more examples of longer streaks from images taken by the Geostationary Ocean Color Imager (GOCI) during three years from 2012 to 2015 and summarized on Table 1. In this area off southern Korea, dredging has been carried out one or twice a week, and during operations, images obtained in a total of 41 different days were available to be analyzed; among them, streak images of plumes appeared 17 times. Interestingly, those plumes appeared with seasonal variability: elongated plume streaks appeared 12 times in 17 images from spring and summer, 4 times in 12 images from autumn and only once in 12 images during winter (Table 1). So, the development of such elongated plume streaks may be seasonally variable, a phenomenon which was previously unknown.

Without any discontinuities such as abrupt changes of current, fronts between the different water bodies, strong lateral velocity gradients by the rivers, a source can produce a continuous streak by the uninterrupted release of a scalar substance. Over a long time and in a large space, discontinuations of the streamlines or water bodies can produce many streaks with various lengths, sizes, and locations. Once such discontinuities occur and those disconnected streaks occupy a whole domain, we can determine macroscopic transport based on this area of occupation of multiple scalar streaks. Transport related with streaks has been intensively studied through theory, as well as numerical and field experiments (e.g., Garret, 2006; Sundermeyer and Price, 1998; Sundermeyer et al., 2005). In the macro-scale view, understanding development of streaks must be the first step to study rather macro-scale dispersion and transport of scalars. Such macro-scale transport has not yet been observed nor studied well, except for field experiments in which dye was released and investigated (Sundermeyer and Price, 1998). Fortunately, the release of fine sediments during the dredging of marine aggregates provided an opportunity to study the initial stage of macro-streak development, despite being a special case. During 8–12 h of dredging, the sediment release can be considered as a continuous source, which is very hard to implement artificially in field experiments. Therefore, the present work collected data in initial-stage plume streaks from satellite images, field measurements, and explain physics by a numerical study.

2. Methods of observation and simulation

The dredging site (34.2°N, 128.4°E) is located about 50 km from the coast of South Korea, which is in the Exclusive Economic Zone (EEZ) of Korea. The mean depth is > 80 m (Fig. 1(a)). Sand mining intermittently took place, usually once or twice a week depending on the weather. We conducted field observations on the 19th of May (late spring) and the 18th of October (late autumn) 2015, while the seabed was being dredged and plumes were forming from the overspilled material. Times when Landsat 8 passed over this area were considered in determining the dates of field measurements. During the field measurements in the spring, Landsat 8 passed over this area and so a satellite image could be acquired (Fig. 1(b)). We also scheduled similarly the field measurement synchronizing with Landsat but a plume was not observed and so we didn't include here for late autumn.

Table 2
Detail descriptions of the instruments and measurements.

Instrument	Measurement variables	Response time (s)	Sampling rate (Hz)	Falling velocity (m/s)	Resolution (m)	Observation period (UTC + 9)
CTD	Conductivity	0.5	4	0.7–0.8	0.18–0.2	Spring: 11:00–15:00
	Temperature	0.5				Autumn: 11:00–17:30
	Pressure	1.0				
OBS	Turbidity	–				
YODA	Conductivity	0.2	10	0.2–0.3	0.02–0.03	
	Temperature	0.2				
	Pressure	0.2				
	Turbidity	–				

Field observations were performed as close as possible to the center of the plume, which was determined from on-the-spot visual observation. Data were collected using a conductivity-temperature-depth sensor (CTD, SBE 19plus, Seabird Electronics), which was also equipped with an optical backscatter sensor (OBS, OBS-3 + , Campbell Scientific). The sampling rates of CTD and OBS were set at 4 Hz and the falling velocity of them was around 0.7–0.8 m/s and so the vertical resolution was about 0.18–0.2 m (Table 2). When data were collected at 5 stations from St.1 (1 km from the source) to St.5 (8 km from the source) with almost 70 m of depth in late spring (Fig. 1(b)), similar sets of data between the stations were also profiled approximately every around 200 m by 40 m of depth using the Yoing Ocean Data Acquisition profiler (YODA, JFE-Advantech), which also equipped with OBS. The vertical resolution of YODA was around 0.02–0.03 m when the falling velocity was adjusted to approximately 0.2–0.3 m/s and the sampling rate was 10 Hz (Table 2). To ensure the reliability of the acquired data from each instrument, post-processing techniques were applied following Thomson and Emery (2014). Temperature and conductivity are realigned with respect to the pressure and minimize the spikes of salinity and density data in CTD and YODA. Finally, the data were smoothed with a low-pass filter at the frequencies of the response time in Table 2. CTD profiled at five stations and YODA sampled continuously between stations for about 4 h in late spring. YODA malfunctioned in October and only CTD was operated for about 6.5 h.

Due to visual limitations at the site, the sediment plume could not be tracked farther downstream than St.5 (Fig. 1(a)), while the image from the satellite shows that the plume extended > 24 km from the source. In autumn, the plume was observed only near the source in the field; moreover satellite images showed no long streaks like those in spring, so data were collected in the vicinity of the source and following the current at similar distances from the source as in the spring. An example set of CTD profiles is presented in Fig. 1(c). Due to its high salinity, warm water was located deeper than cold water in the mixing zone of the pycnocline (Fig. 1(c)), so water column conditions were favorable to double diffusive convection; but the current was strong enough to remove significant effects of diffusive convection on this mixing zone.

To understand and validate the observed processes, the excessively elongated sediment plume streaks were also numerically simulated with the Regional Ocean Modeling System (ROMS), which can solve the three-dimensional, finite-difference approximations, free-surface, primitive equations with stretched terrain-following vertical s-coordinates and curvilinear horizontal coordinates based on the hydrostatic and Boussinesq approximations (Haidvogel et al., 2000; Warner et al., 2008). ROMS can also include a sediment-transport module of non-cohesive sediment classes, each with its own grain diameter, density, and settling velocity. The equations of sediment transport for each sediment size are given by Blaas et al. (2007) and Warner et al. (2008):

$$\frac{\partial c_j}{\partial t} + \frac{\partial u_i c_j}{\partial x_i} + \frac{\partial}{\partial x_i}\left(K_i \frac{\partial c_j}{\partial x_i}\right) - w_{s,j}\frac{\partial c_j}{\partial x_3} = C_{source,j}. \quad (1)$$

Here, the subscript i is coordinate direction with x_3 vertically upward; K_i is the eddy diffusivity; c_j represents sediment concentration of sediment class j; $w_{s,\ j}$ is the vertical settling velocity; and $C_{source,\ j}$ represents a point source releasing at the surface.

ROMS solves the horizontal advection equations with the 3rd-order upstream bias scheme and then expands the horizontal solution to the vertical direction with the 4th-order centered scheme. For scalars, the 3rd-order upstream horizontal advection is used (Hedstrom, 2009). The 3rd-order Adams-Bashforth (AB3) integrates the horizontal momentum solutions temporally and the leapfrog predictor with a two time trapezoidal (LF-TR) scheme integrates the solution of tracers (Warner et al., 2008; Hedstrom, 2009).

Sediments were released at the location 34.2°N, 128.4°E where the mining activity occurred. In numerical simulation, we released sediments much shorter time than the duration of dredging to capture the plume behavior and mechanism clearly rather than realize the operation. Temperature and salinity of the released mixture were same as those measured at the bottom, since the water and sediments were delivered from the bottom to the surface through a pipe without mixing with the surrounding waters. The released mixtures include two sizes of sediments; one is sand with 0.125 mm radius and another is mud with 0.024 mm radius and the densities are assumed to be same with value of 2650 kg/m^3. In the model, the settling velocity is constant with value of 9.4 mm/s for sand and 0.4 mm/s for mud, which were determined by the empirical function of grain size (Soulsby, 1997, Blaas et al., 2007).

The equation of state for seawater density is defined with a function of temperature, salinity, and total pressure. Since suspended sediments can also affect total density of mixtures and water column, total density is account for the weight of each sediment class in the equation of state as bellow:

$$\rho = \rho_{water} + \sum_{m=1}^{N_{sed}} \frac{C_{s,m}}{\rho_{s,m}}(\rho_{s,m} - \rho_{water}), \quad (2)$$

where ρ_{water} and $\rho_{s,\ m}$ are the densities of water and sediments respectively and $C_{s,\ m}$ is suspended sediment concentration of each sediment class of N_{sed}, here we have two classes of sand and mud. Such an additional equation can enable the model to simulate processes when the sediment density influences hydrodynamics (Warner et al., 2008). ROMS employs a piecewise parabolic method (Colella and Woodward, 1984) and a weighted essentially non-oscillatory scheme (Liu et al., 1994) to solve the vertical advection.

Outputs from a global model were one-way nested in two steps to avoid the effect of spatial resolution differences between global and regional models (Pham et al., 2016). The global model (HYCOM) provides the oceanic variables such as temperature, salinity, horizontal momentum, and sea surface height on a 1/12° × 1/12° (≈9 km) grid, discretized vertically with 33 layers and updated every 24 h. Such results were compared and validated with the observational and other model results as Hurlburt et al. (2009), Chu et al. (2001), and Liu and Chai (2009). In comparison between results of ROMS and HYCOM, the correlation coefficients of temperature and salinity are about 0.75 and 0.6, respectively. In the first downscaling, a 1.2 km × 1.2 km grid cell is used for simulation of the larger domain ranging from 127.50°E to

130.50°E longitude and 33.50°N to 35.20°N latitude, equivalent to the lengths 288 km and 234 km, respectively. In the second downscaling, a resolution of 300 m × 300 m simulates the domain of interest ranging from 128.15°E to 128.90°E and 33.97°N to 34.43°N, equivalent to 75 km and 60 km, respectively (Fig. 1(a)). The current speed is around 0.3 m/s and the major direction of currents is northeast which are similar to Chang et al. (2004). Tidal data are downloaded from TPXO7.2 and provided for eight primaries (M2, S2, N2, K2, O1, P1, Q1), two long-periods (Mn, Mm) and 3 non-linear (M4, MS4, MN4) harmonic constituents. Tidal data has about 0.93 of the correlation with the data obtained from the Geoje tidal station installed near the study area. The M2 dominates among all tidal constituents (Odamaki, 1989) in this region and its magnitudes and directions agree well with the results of Park et al. (2006). The bathymetries are extracted from ETOPO1, which is a global, integrated bathymetric-topographic, digital elevation model with a cell size of 1 arc-minute (Amante and Eakins, 2009). For turbulence closure, an eddy diffusivity model is used with *K*-profile parameterization (Large et al., 1994).

The coupling atmospheric data for the ROMS input were downscaled from the NCEP final operational global analysis data (NCEP-FNL) by using Weather Research Forecast model (WRF). The NCEP-FNL supplies data on every 1° × 1° grid and updates them every 6 h. The domain of WRF model is greater than that of the ocean model but the resolution of the WRF is nearly same to that of the ocean model in order to minimize the errors due to the atmosphere forcing. The main atmospheric variables include air temperature, pressure, relative humidity, net short and long wave heat fluxes and winds at 10 m.

3. Results and discussion

During mining operations, the plume of suspended sediment was clearly observed in a spring satellite image (Fig. 1(b)). Plume streaks extended > 24.4 km downstream from the dredging location and had moved about 7.5 km laterally on the 19th of May (late spring). In contrast to the spring image, we could not find any streak of the plume in the satellite image from the 18th of October (late autumn). Just as the images were different from each other, the measured temperature, salinity, and density profiles also differed in the two seasons (Fig. 2(a)). While the mean density was higher in spring than in autumn, the density difference between the upper and lower layers in spring was around 1.7 kg/m^3, which is 1.8 kg/m^3 smaller than in autumn. Therefore, the stratification was stronger in the autumn than in the spring. Also, strong mixing at the water surface occurs in autumn and in winter, so the surface mixed layer was thicker in autumn and winter than in spring and summer. Due to weaker stirring in spring, the surface mixed layer developed to a depth of about 17 m, where the pycnocline began (Fig. 2(b)); this was 11 m shallower than 28 m of the surface mixed layer in autumn (Fig. 2(c)). Such seasonally varying density structures significantly affect the turbidity distribution. In both seasons, turbidities were detectable at depths shallower than 40 m (Fig. 2(b) and (c)). In spring relatively high turbidity was still observed at 40 m and maximum turbidity was found at depths shallower than 20 m (Fig. 2(b)), while in autumn turbidities at depths shallower than 40 m, were nearly uniform and very close to the sensor's minimum detectable level, suggesting that most of the sediments had already sunk beyond 40 m depth (Fig. 2(c)).

Table 3 shows the significant wave heights and directions, wind speeds and directions of the last five years provided by the Korea Meteorological Administration (KMA, 2017). Wind blows mainly to the southeast direction in spring, summer, and autumn and the southwest direction in winter. Especially in winter, since the magnitudes of wind were larger than the other seasons and the directions of wind were opposite to the direction of the surface current in this region (Chang et al., 2004), the surface mixed layer developed deeply near winter seasons including the late autumn. Waves have propagated to the southwest over whole years and the significant wave heights in autumn and winter are slightly larger than in spring and summer (Table 3). Therefore, the stronger surface mixings are expected in autumn and winter. However, it is necessary to consider the complicated nonlinearities such as wave breakings, which generate turbulence and entrains air bubbles into the deeper location (Weber, 2008; Qiao and Huang, 2012).

Two main factors determine whether a plume can develop in the form of an elongated streak. One is the background mixing and another is the restoring force from negative buoyancy of the released water. When background processes such as waves, current, and shear are strong, as in autumn, they can deepen the surface mixed layer and also well mix vertically the suspended sediments (Fig. 2(c)). Vertical stratification itself could directly affect the falling speed of coarse particles, but finer sediment behaves more like a passive scalar. If a water body does not sink, then fine sediments in the water body also do not sink, as seen in spring (Fig. 2(b)). The evolution of a surface plume then depends on background mixing processes near the surface rather than stratification in the lower pycnocline. The other factor, the restoring force, is determined by the density of the mixture after being discharged from the barge. Assuming similar amounts of surface and bottom waters are mixed after discharge, the mixed water descends to a depth where water with the same density as the mixed water is found. In the spring, such an equivalent density is found around 25 m below the surface, but in autumn, this depth is located around 49 m below the surface, much deeper than in spring. In autumn, the restoring force produced by the larger density difference is stronger, so the mixed

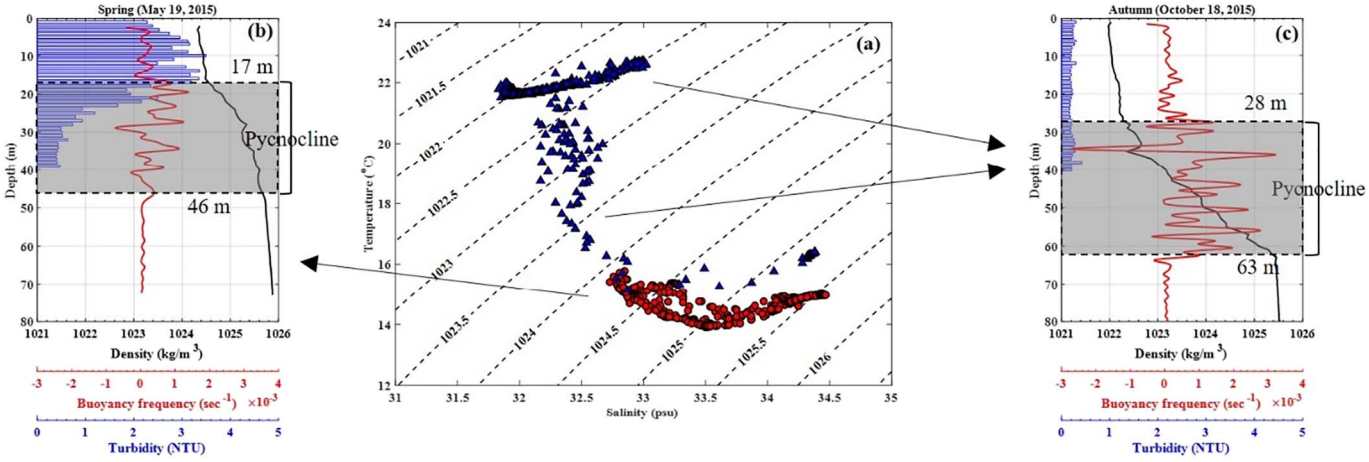

Fig. 2. (a) T-S diagram for late spring (May 19, 2015; red dots) and late autumn (October 18, 2015; blue triangles). Vertical profiles of density, buoyancy frequency and turbidity are shown for spring (b) and autumn (c).

Table 3
Seasonal variability of wind and wave in recent 5 years.

	Spring				Summer				Autumn				Winter			
	Wind		Wave		Wind		Wave		Wind		Wave		Wind		Wave	
	Speed (m/s)	Direction (°)	Speed (m/s)	Direction (°)	Speed (m/s)	Direction (°)	Speed (m/s)	Direction (°)	Speed (m/s)	Direction (°)	Speed (m/s)	Direction (°)	Speed (m/s)	Direction (°)	Speed (m/s)	Direction (°)
2012	6.44	163.10	1.10	206.82	6.12	133.19	1.13	218.21	5.99	138.83	1.05	210.01	7.02	222.45	1.11	227.42
2013	5.78	179.53	1.03	189.59	4.74	175.30	0.88	201.72	6.62	136.79	1.21	206.38	6.61	204.52	1.11	224.08
2014	5.42	172.33	0.95	192.87	5.50	143.09	1.02	210.66	6.28	126.97	1.09	213.84	7.06	184.44	1.27	212.54
2015	5.38	171.91	0.90	192.62	5.08	153.52	1.01	187.76	6.58	135.15	1.20	199.38	6.52	213.59	1.08	213.04
2016	5.34	155.80	0.99	180.70	4.79	166.32	0.89	154.94	6.63	108.90	1.20	188.64	6.59	205.69	1.07	201.07
Mean	5.67	168.53	0.99	192.52	5.24	154.28	0.99	194.66	6.42	129.33	1.15	203.65	6.76	206.14	1.13	215.63

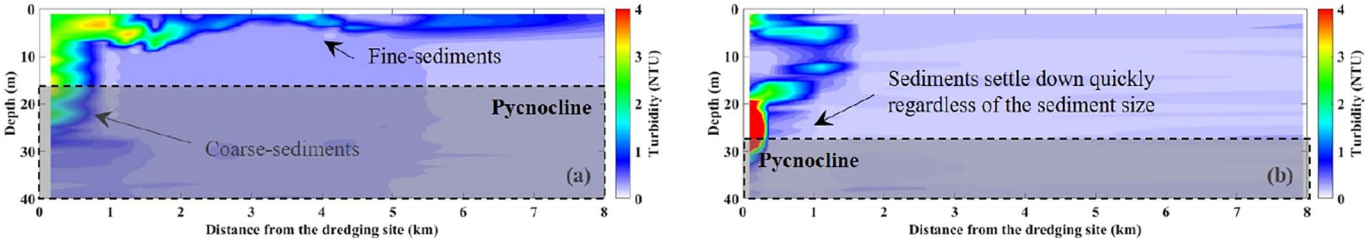

Fig. 3. Vertical distribution of turbidity (NTU) in (a) late spring (May 19, 2015) and (b) late autumn (October 18, 2015) downstream of the dredging site.

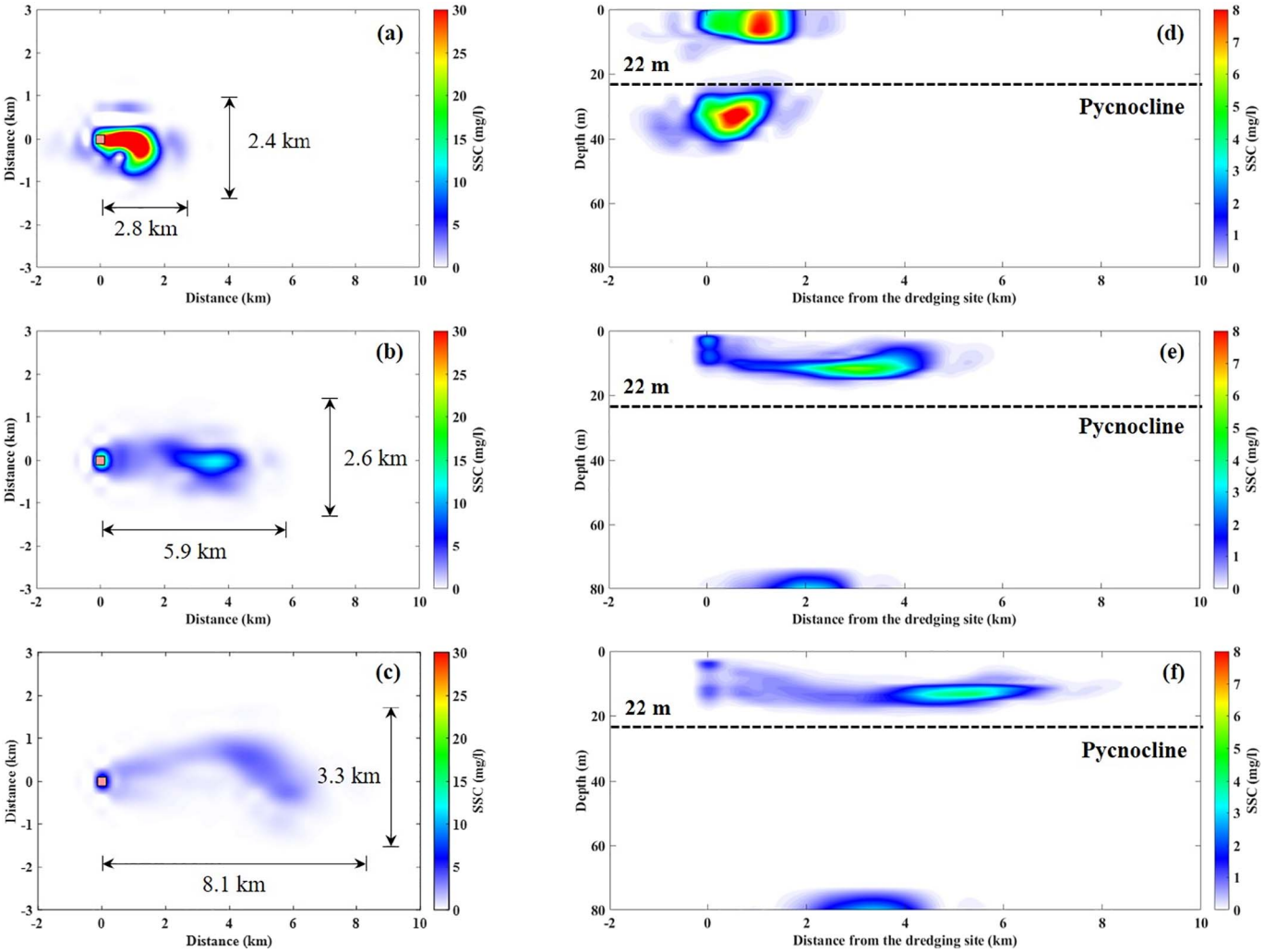

Fig. 4. Horizontal distribution of simulated total sediment concentration (mg/l) after (a) 1 h, (b) 3 h, and (c) 5 h and vertical distribution of simulated total sediment concentration (mg/l) after (d) 1 h, (e) 3 h, and (f) 5 h, in late spring.

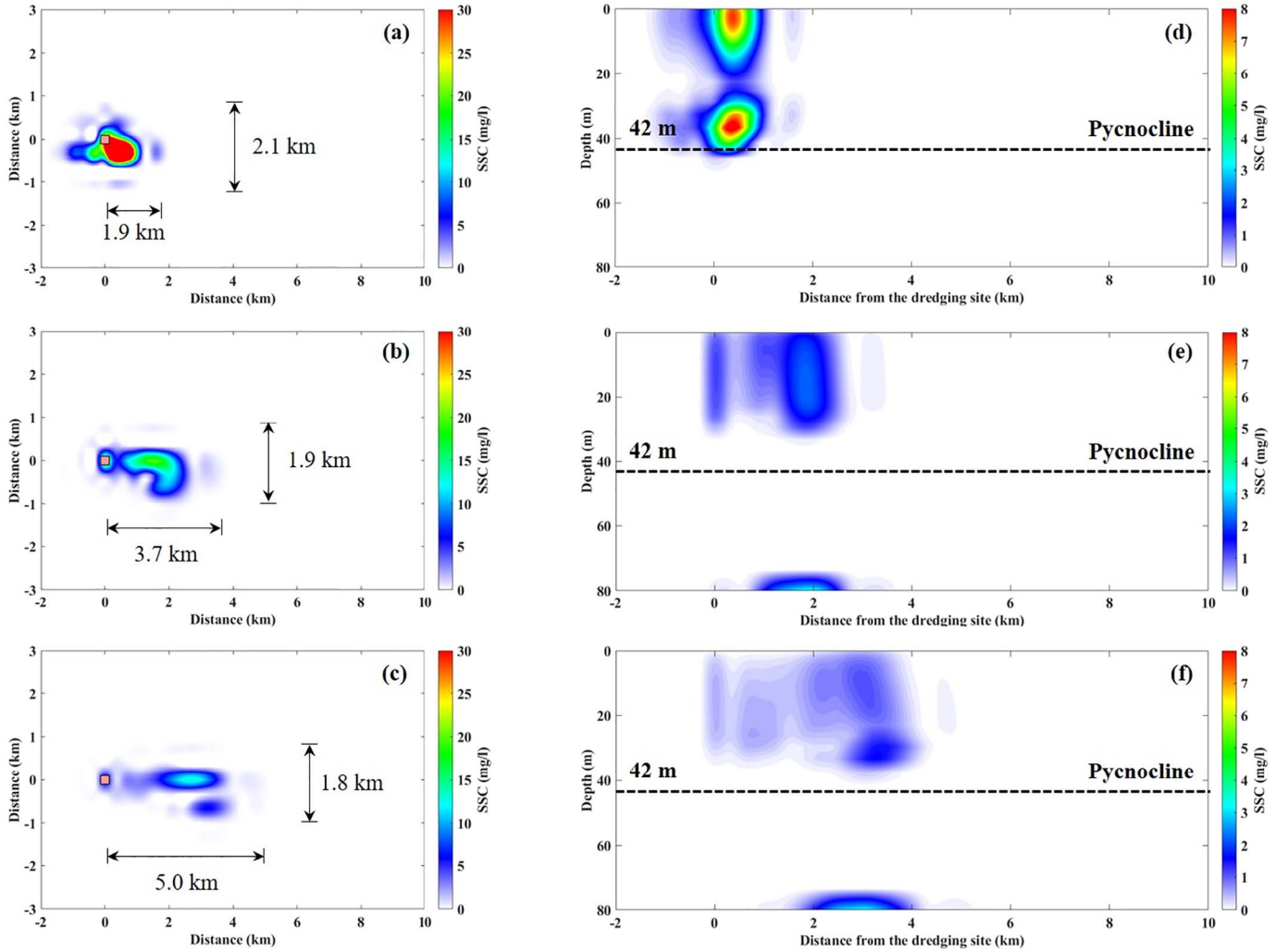

Fig. 5. Same as Fig. 4, but for late summer.

water descends faster and deeper than in spring. The strong restoring force reduces the total available amount of suspended sediments to be transported in horizontal directions, and thus reduces the length of a plume developing downstream. Such processes are clearly observed in Fig. 3, which shows along-sectional distributions of the suspended sediment concentration downstream of the dredging site. Concentrations were measured from a ship in the field following the plume. In the spring, a long plume developed, with over 8 km length and 10 m thickness (Fig. 3(a)); such a plume was not observed in the autumn (Fig. 3(b)). As discussed, in spring the mixed zone was not thick enough to indicate vigorous vertical mixing, so finer suspended sediments could form a plume streak at the surface. But in autumn, a long streaked image of the plume was not seen and much higher concentrations of sediments were observed near the dredging point (Fig. 3(b)) in the deeper locations, indicating rapid descent of the sediments. This is because the mixed zone was well developed indicating vigorous vertical mixing of sediments, so only small amounts of sediment could travel downstream.

Numerical simulation produced results similar to our observations and helped us understand the processes involved. In late spring the sediment plume extended far downstream from the sediment-release location within 20 m of water depth (Fig. 4). 1 h after the sediment mixture was released, a plume appeared but did not form a streak (Fig. 4(a)) and no coarse sediments had yet sunk to the bottom (Fig. 4(d)). After 3 h, coarse sediments had sunk near the bottom and a plume of finer sediments formed a streak in the downstream direction of the background current (Fig. 4(b) and (e)) within 22 m of pycnocline depth. Even after 5 h, the sediment plume stayed near the surface and formed a long streak extending about 8.1 km downstream and meandering cross-stream about 3.3 km (Fig. 4(c) and (f)). In the present simulation, the behavior of the plume water body was not significantly influenced by the sediments but only by the density of water itself. While coarse sediments descended separately from the plume, finer particles followed the water-body flow. Hence the plume of fine sediments could travel over long distances and times by advection in the absence of strong mixing and vertical restoring force.

In late summer, at 1 h after releasing the mixtures (Figs. 4(a) and 5(a)), the length of sediment plume is slightly shorter than that in the late spring and the vertical distribution of suspended sediments is very similar to that in the late spring with the separation of finer and coarser sediments (Figs. 4(d) and 5(d)). At 3 h after releasing, late spring and late summer show the horizontal distribution of sediments (Fig. 4(b) and (e)). In late spring, a streak of the plume developed well (Fig. 5(b)) but in late summer, the streak was not elongated well but the large amount of sediments were settling down within the mixed layer, which is just above the pycnocline (Fig. 5(e)). In late summer, after 5 h, most of sediments fell down by above 42 m and were diluted (Fig. 5(f)).

In late autumn, 1 h after releasing the mixtures, the horizontal distribution of sediments looks similar to that in late spring (Figs. 4(a), 5 (a), and 6 (a)). But unlike the May or late spring (Fig. 4(d)) and early autumn (Fig. 5(d)), fine and coarse sediments were not separated from each other (Fig. 6(d)) during descent, with fine sediments also sinking

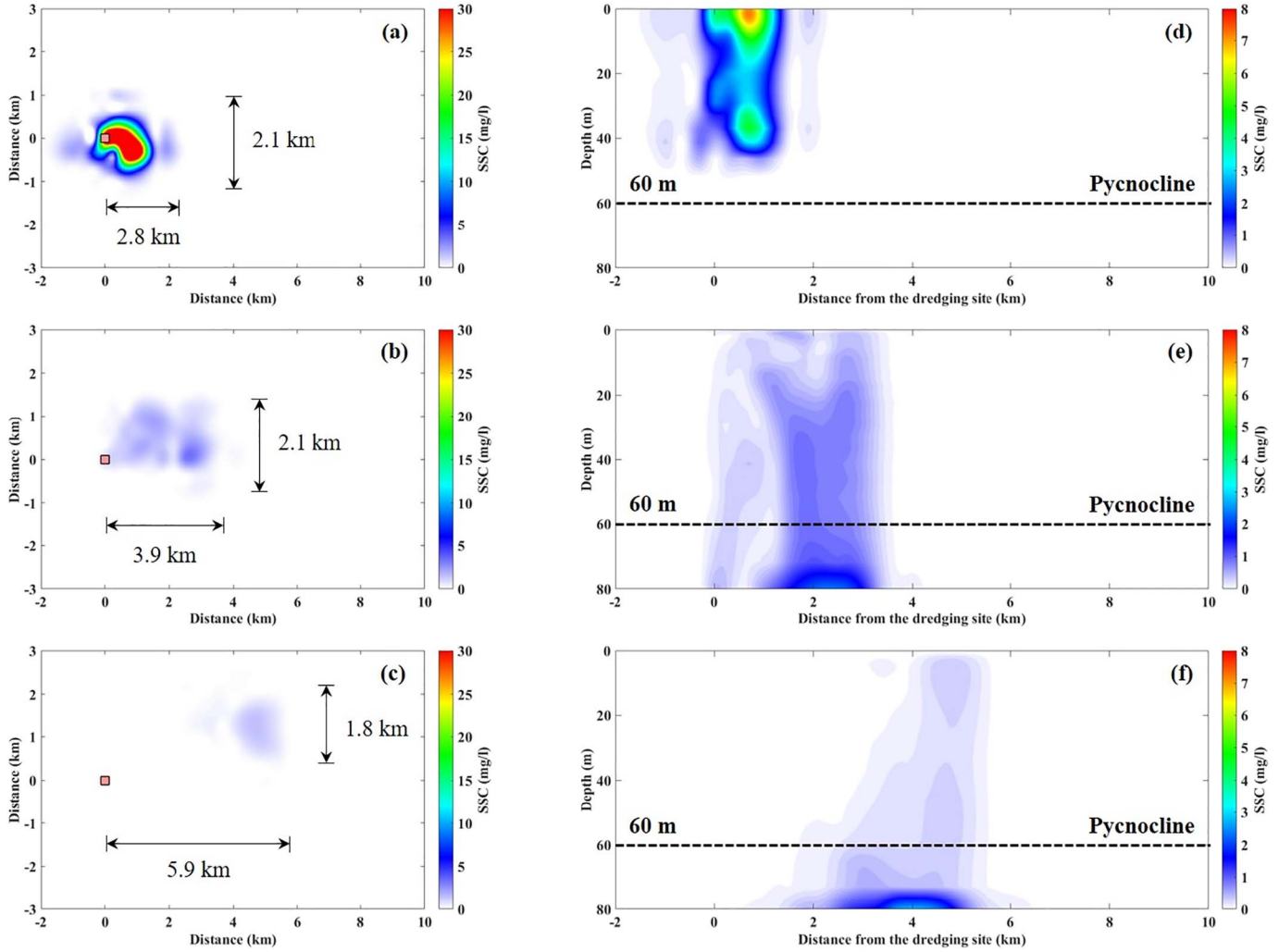

Fig. 6. Same as for Figs. 4 and 5, but for late autumn.

Table 4
Restoring force and depth of the pycnocline obtained from the numerical model.

	Middle spring - April	Late spring - May	Early autumn - Sepember	Late autumn - October
Restoring force (N/m^3)	0.0530	0.0186	0.0765	0.1246
Pycnocline (m)	28	22	42	60

to the bottom quickly due to the very deep mixed layer (i.e. same to very deep pynocline) and the restoring force from the mixture's negative buoyancy acting on the mixed layer (Fig. 6(d)). Both sediments type sank together to the bottom in late autumn, and after just 3 h, sediments at the water surface were much diluted to a low concentration (Fig. 6(b)). After 5 h, only very dilute sediments were observed at the water surface 5.9 km downstream from the sediment-release location (Fig. 6(c)); most of the sediments had sunk to the bottom, although dilute fine sediments were observed throughout the water column (Fig. 6(f)).

The restoring forces are determined in four cases. This restoring force was determined after the releasing and collect 1 h later (simulation) when the released water mixed enough with the background and the coarser sediments somehow fell down separately from the suspended sediments so they do not generate a convective flow any longer. The restoring forces were quantified with the difference between densities of the released and the background water as follow:

$$F_{restoring} = \Delta\rho g = (\rho_r - \rho_b)g, \quad (3)$$

where g is the gravitational acceleration, ρ_b is the density of the surface background water, and ρ_r is the density of the released mixture. The density of the released mixtures was obtained at the surface layer of the mining site after released and the density of the surface background water was sampled at the far upstream from the mining site. Table 4 summarized the restoring forces obtained from the numerical model which were quantified by the above equation and the depths where pycnoclines begin developing and, respectively. As in table, restoring force of spring is much smaller than autumn. In particular in late spring, the restoring force is 6 times smaller than late autumn and much smaller than any other cases. Along with the small restoring force, pycnocline begins developing in the shallower depth, 22 m (Table 4, Fig. 4) while in late autumn that was very deep at 60 m (Table 4, Fig. 6). Early spring or winter and late summer show the similar range of the restoring forces, the plume shapes and structures even though we didn't include early spring's figure. This is consistent with the fact that the mixed layer thickness and the restoring forces have strong seasonal variations and so their seasonality differs the horizontal transport of the suspended sediments.

4. Conclusions

There have been numerous reports regarding the dependency of

sediment suspension and transport on the ambient hydrodynamic processes. Mean currents mainly determine the horizontal and vertical transport rates of suspended sediments (Blaas et al., 2007; Wit et al., 2014). Also local perturbations such as waves and shear can control the amount of sediment available for horizontal transport (Blaas et al., 2007): when vertical mixing is strong, suspended sediments are diluted and the amount available to be transported horizontally decreases. Therefore, gradients of velocity and density, which control turbulence, are critical in determining horizontal transport of suspended sediments. They can also be influenced by local atmospheric weather conditions such as wind, solar radiation and rain, and by local oceanic hydrodynamic conditions such as waves and tides (Moum and Smyth, 2001; Xu et al., 2002; Blaas et al., 2007).

In the case of sediment-water mixtures discharged during sand mining, along with conventionally introduced determinants of horizontal transport, a negative-buoyancy force causing denser water and sediments to sink must play an important role as it does in providing the restoring force governing internal waves. Mixtures of seawater and aggregates pumped from the bottom are generally cold, saltier and hence denser than the surface water and so have a downward restoring force. In these the mixtures, discharged into the surrounding surface seawater, coarser sediments sink rapidly as in a descending thermal (Tsang, 1971; Li, 1997; Noh, 2000) while finer components sink slowly, mixing with the ambient waters and composing a plume of suspended particles. Thus finer components are essentially carried along with the seawater as water particles.

When the water column has a large density difference between surface and bottom, and the bottom water is dredged and brought to the surface, this bottom water is acted on by a strong restoring force at the surface, which can rapidly sink the mixture of water and suspended fine sediments along with the coarser components. But, when the water-column density difference is small, the released plume has only a small restoring force, and this plume of suspended sediments will float at the surface without sinking appreciably. In particular, when the surface water is not strongly stirred by waves and neither sheared nor stretched by velocity gradients, such a plume floating on the surface will be observed by a satellite to travel over a long distance as a plume resembling a streak.

During marine-aggregate mining operations, sediment-water mixtures dredged from the seabed mix again with the surface water. In spring, at the present observational location, the density of these mixed waters differs little from that of the surrounding surface water, since the density difference between surface and bottom waters is small. In other words, the plume can be suspended at the surface without sinking. Also, at this location in spring or summer, weather is generally much calmer than in autumn or winter (Table 3), so waves and turbulence in the surface layer are not strong. These conditions differ from those of riverine transport, because the open ocean generally lacks strong horizontal shears resulting from boundaries or bottom effects. Hence when fine sediments are brought from the bottom to the sea surface in spring, or under similar conditions, they do not vigorously disperse horizontally but instead form a streaked plume. Until such a plume travels into a new domain having strong shears or turbulence, it persists in the form of a streak.

Acknowledgements

This research was supported by “Study on coastal marine ecosystem structures and suspended sediment in the EEZ sand mining of Korean coastal waters” funded by K-Water (No. 0415-20140153) and the National Research Foundation of Korea (NRF) Grant (No. 2017R1A2B400797) funded by MSIP of Korea. All data can be provided with requesting to the corresponding author.

References

Ali, K., Ortiz, J., Bonini, N., Shuman, M., Sydow, C., 2016. Application of aqua MODIS sensor data for estimating chlorophyll a in the turbid case 2 waters of Lake Erieusing bio-optical models. GISci. Remote Sens. 53, 483–505.

Amante, C., Eakins, B.W., 2009. Etopo1 1 arc-minute global relief model: procedures, data sources and analysis. NOAA technical memorandum NESDIS NGDC-24. http://www.ngdc.noaa.gov/mgg/global/global.html.

Battisto, G.M., Friedrichs, C.T., 2003. Monitoring suspended sediment plume formed during dredging using ADCP, OBS, and bottom samples. In: Proceedings of the Conference on Coastal Sediments. American Society of Civil Engineers (12 pp.).

Blaas, M., Dong, C.M., Marchesiello, P., McWilliams, J.C., Stolzenbach, K.D., 2007. Sediment transport modeling on southern Californian shelves: a ROMS case study. Cont. Shelf Res. 27, 832–853.

Capello, M., Cutroneo, L., Ferranti, M., Budillon, G., Bertolotto, R., Ciappa, A., Cotroneo, Y., Castellano, M., Povero, P., Tucci, S., 2013. Simulations of dredged sediment spreading on a Posidonia oceanic meadow off the Ligurian coast, northwestern Mediterranean. Mar. Pollut. Bull. 79, 196–204.

Chang, K.I., Teague, W.J., Lyu, S.J., Perkins, H.T., Lee, D.K., Watts, D.R., Kim, Y.B., Mitchell, D.A., Lee, C.M., Kim, K., 2004. Circulation and currents in the southwestern East/Japan Sea: overview and review. Prog. Oceanogr. 61, 105–156.

Chu, P.C., Land, J., Fan, C.W., 2001. Japan Sea thermohaline structure and circulation. Part I: climatology. J. Phys. Oceanogr. 31, 244–271.

Colella, P., Woodward, P., 1984. The piecewise parabolic method (PPM) for gas-dynamical simulations. J. Comput. Phys. 54, 174–201.

Erftemeijer, P.L., Lewis III, R.R.R., 2006. Environmental impacts of dredging on seagrasses: a review. Mar. Pollut. Bull. 52, 1553–1572.

Garret, C., 2006. Turbulent dispersion in the ocean. Prog. Oceanogr. 70, 113–125.

Goodwin, C.R., Michaelis, D.M., 1984. Appearance and Water Quality of Turbidity Plumes Produced by Dredging in Tampa Bay, Florida. U.S. Geological Survey Water-supply Paper 2192. Reston, Virginia.

Haidvogel, D.B., Arango, H.G., Hedstrom, K., Beckmann, A., Mananotte-Rizzoli, P., Shchepetkin, A.F., 2000. Model evaluation experiment in the North Atlantic Basin: simulations in nonlinear terrain-following coordinates. Dyn. Atmos. Oceans 32, 239–281.

Hedstrom, K.S., 2009. Draft Technical Manual for a Coupled Sea-ice/ocean Circulation Model (Version 3). U.S. Department of the Interior Minerals Management Service Anchorage, Alaska (Contract No. M07PC13368).

Hitchcock, D.R., Drucker, B.R., 1996. Investigation of benthic and surface plumes associated with marine aggregates mining in the United Kingdom. Oceanol. Int. 2, 221–234.

Hurlburt, H.E., Brassington, G.B., Drillet, Y., Kamachi, M., Benkiran, M., Badie, R.B., Chassignet, E.P., Jacobs, G.A., Galloudec, O.L., Lellouche, J.M., Metzger, E.J., Oke, P.R., Pugh, T.F., Schiller, A., Smedstad, O.M., Tranchant, B., Tsujino, H., Usui, N., Wallcraft, A.J., 2009. High resolution global and basin scale ocean analyses and forecasts. Oceanography 22 (3), 80–97.

Kim, C.S., Lim, H.S., 2007. Safety criteria on water depth, offshore distance and dredging volume in marine sand mining operation in Kyunggi Bay, Korea. J. Coast. Res. SI50, 507–510.

Kim, C.S., Lim, H.S., 2009. Sediment dispersal and deposition due to sand mining in the coastal waters of Korea. Cont. Shelf Res. 29, 194–204.

Kim, Y., Im, J., Ha, H., Choi, J., Ha, S., 2014. Machine learning approaches to coastal water quality monitoring using GOCI satellite data. GISci. Remote Sens. 51, 158–174.

KMA, 2017. Monthly report of marine data. Korea Meteorological Administrationhttp://www.weather.go.kr/weather/climate/data_sea.jsp.

Kutser, T., Metsamaa, L., Vahtmäe, Ë., Aps, R., 2007. Operative monitoring of the extent of dredging plumes in coastal ecosystems using MODIS satellite imagery. J. Coast. Res. SI 50, 180–184.

Large, W.G., McWilliams, J.C., Doney, S.C., 1994. Ocean vertical mixing: a review and a model with a nonlocal boundary layer parameterization. Rev. Geophys. 32 (4), 363–403.

Li, C.W., 1997. Convection of particle thermals. J. Hydraul. Res. 35 (3), 363–376.

Liu, F., Chai, F., 2009. Seasonal and inter-annual variation of physical and biological processes during 1994–2001 in the Sea of Japan/East Sea: a three-dimensional physical-biogeochemical modeling study. J. Mar. Syst. 79, 265–277.

Liu, X.D., Osher, S., Chen, T., 1994. Weighted essentially non-oscillatory schemes. J. Comput. Phys. 115, 200–212.

Moum, J.N., Smyth, W.D., 2001. Upper ocean mixing processes. In: Encyclopedia of Ocean Sciences. 6. Academic Press, pp. 3093–3100.

Newell, R.C., Seiderer, L.J., Hitchcock, D.R., 1998. The impact of dredging works in coastal waters: a review of the sensitivity to disturbance and subsequent recovery of biological resources on the seabed. Oceanogr. Mar. Biol. Annu. Rev. 36, 127–178.

Noh, Y., 2000. Sedimentation of a particle cloud across a density interface. Fluid Dyn. Res. 27, 129–142.

Odamaki, M., 1989. Co-oscillating and independent tides of Japan Sea. J. Oceanogr. Soc. Jpn 45, 217–232.

Park, J.H., Watts, D.R., Wimbush, M., 2006. Rapid variability in the Japan/East Sea: basin oscillations internal tidal and near-inertial oscillations. Oceanography 19, 76–85.

Pham, V.S., Hwang, J.H., Ku, H., 2016. Optimizing dynamic downscaling in one-way nesting using a regional ocean model. Ocean Model 106, 104–120.

Qiao, F., Huang, C.J., 2012. Comparison between vertical shear mixing and surface wave-induced mixing in the extratropical ocean. J. Geophys. Res. 117 (C00J16). http://dx.doi.org/10.1029/2012JC007930.

Son, S., Kim, Y., Kwon, J., Kim, H., Park, K., 2014. Characterization of spatial and temporal variation of suspended sediments in the Yellow and East China Seas using

satellite ocean color data. GISci. Remote Sens. 51, 212–226.
Soulsby, R.L., 1997. Dynamics of Marine Sands. Thomas Telford, London.
Sundermeyer, M.A., Price, J.F., 1998. Lateral mixing and the North Atlantic tracer release experiment: observation and numerical simulations of Lagrangian particles and a passive tracer. J. Geophys. Res. 103, 21,281–21,297.
Sundermeyer, M.A., Ledwell, J.R., Oakey, N.S., Greenan, J.W., 2005. Stirring by small-scale vortices caused by patchy mixing. J. Phys. Oceanogr. 35, 1245–1262.
Thomson, R.E., Emery, W.J., 2014. Data Analysis Methods in Physical Oceanography, 3rd edn. Elsevier Science, Amsterdam.
Tsang, G., 1971. Laboratory study of line thermals. Atmos. Environ. 5, 445–471.
Warner, J.C., Sherwood, C.R., Signell, R.P., Harris, C.K., Arango, H.G., 2008. Development of a three dimensional, regional, coupled wave, current, and sediment transport model. Comput. Geosci. 34, 1284–1306.
Weber, J.E.H., 2008. A note on mixing due to surface wave breaking. J. Geophys. Res. 113, C11009. http://dx.doi.org/10.1029/2008JC004758.
Wit, L.D., Talmon, A.M., Rhee, C.V., 2014. 3D CFD simulation of trailing suction hopper dredger plume mixing: a parameter study of near field conditions influencing the suspended sediment source flux. Mar. Pollut. Bull. 88, 47–61.
Xu, J.P., Noble, M., Eittreim, S.L., 2002. Suspended sediment transport on the continental shelf near Davenport, California. Mar. Geol. 181, 171–193.